

ORIGINAL ARTICLE

Pathogenicity of a novel missense variant associated with choroideremia and its impact on gene replacement therapy

Simona Torriano^{1,2,†}, Nejlja Erkilic^{1,2,†}, Valérie Faugère³, Krishna Damodar^{1,2}, Christian P. Hamel^{1,2,4,5}, Anne-Francoise Roux^{3,6} and Vasiliki Kalatzis^{1,2,*}

¹Inserm U1051, Institute for Neurosciences of Montpellier, Montpellier, France, ²University of Montpellier, Montpellier, France, ³Laboratory of Molecular Genetics, CHRU, Montpellier, France, ⁴Department of Ophthalmology, CHRU, Montpellier, France, ⁵Centre of Reference for Genetic Sensory Diseases, CHRU, Montpellier, France and ⁶Laboratory of Rare Genetic Diseases, EA 7402, University of Montpellier, Montpellier, France

*To whom correspondence should be addressed at: Inserm U1051, INM, Hôpital St Eloi, BP 74103, 80 Avenue Augustin Fliche, 34091 Montpellier, France. Tel: +33 499636076; Fax: +33 499636020; Email: vasiliki.kalatzis@inserm.fr

Abstract

Choroideremia (CHM) is an inherited retinal dystrophy characterised by progressive degeneration of photoreceptors, retinal pigment epithelium (RPE) and underlying choroid. It is caused by loss-of-function mutations in *CHM*, which has an X-linked inheritance, and is thus an ideal candidate for gene replacement strategies. *CHM* encodes REP1, which plays a key role in the prenylation of Rab GTPases. We recently showed that an induced pluripotent stem cell (iPSc)-derived RPE model for CHM is fully functional and reproduces the underlying prenylation defect. This criterion can thus be used for testing the pathogenic nature of novel variants. Until recently, missense variants were not associated with CHM. Currently, at least nine such variants have been reported but only two have been shown to be pathogenic. We report here the characterisation of the third pathogenic missense *CHM* variant, p.Leu457Pro. Clinically, the associated phenotype is indistinguishable from that of loss-of-function mutations. By contrast, this missense variant results in wild type *CHM* expression levels and detectable levels of mutant protein. The prenylation status of patient-specific fibroblasts and iPSc-derived RPE is within the range observed for loss-of-function mutations, consistent with the clinical phenotype. Lastly, considering the current climate of CHM gene therapy, we assayed whether the presence of mutant REP1 could interfere with a gene replacement strategy by testing the prenylation status of patient-specific iPSc-derived RPE following AAV-mediated gene transfer. Our results show that correction of the functional defect is possible and highlight the predictive value of these models for therapy screening prior to inclusion in clinical trials.

Introduction

Inherited retinal dystrophies (IRDs) are a large group of clinically and genetically heterogeneous disorders (1) that are

characterised by a degeneration of the outer retina that leads to progressive vision loss. The age of onset of legal blindness depends on the disease. The majority of these disorders are due to loss-of-function mutations with a recessive or X-linked

[†]These authors contributed equally to the work.

Received: May 4, 2017. Revised: June 16, 2017. Accepted: June 19, 2017

© The Author 2017. Published by Oxford University Press. All rights reserved. For Permissions, please email: journals.permissions@oup.com

inheritance, making them ideal candidates for gene replacement strategies (2). This was confirmed by the first clinical trials for Leber congenital amaurosis, due to mutations in the *RPE65* gene (3,4). Subsequent clinical trials were performed for retinitis pigmentosa, due to mutations in the *MERTK* gene (5), and choroideremia due to mutations in the *CHM* gene (6).

Choroideremia (CHM) is an X-linked IRD characterised by a progressive degeneration of the photoreceptors, retinal pigment epithelium (RPE) and underlying choroid. Clinically, affected individuals present with night blindness in childhood and, due to progressive loss of the visual field, legal blindness by 40 to 50 years of age (7). CHM has a prevalence of 1/50 000 to 1/100 000 and is due to mutations in the gene *CHM* that encodes Rab Escort Protein 1, REP1 (8). REP1 plays a key role in the prenylation of Rab guanosine triphosphatases (GTPases), which is a vital process for their role as regulators of vesicular transport (9). We recently generated an induced pluripotent stem cell (iPSc)-derived RPE model for CHM and showed that the patient-specific iPSc-derived RPE is fully functional and reproduces the prenylation defect of the disease (10). This functional criterion can thus be exploited for testing the pathogenic nature of novel variants.

A large number of *CHM* mutations have been reported to date (see the Locus Specific Database https://grenada.lumc.nl/LOVD2/Usher_montpellier/home.php; date last accessed June 16, 2017). The majority of these are loss-of-function mutations including nonsense mutations, small or large exon deletions, and splice site mutations (7). Nonsense mutations are associated with the disease at a particularly high frequency (11,12). These types of *CHM* alterations result in the absence of REP1 or a premature termination of translation leading to an unstable protein. Until recently, missense variants were not associated with the disease and to this day are rare. The first such mutation, described in 2009, is p.Leu550Pro (L550P) and it results in a low level of REP1 expression (13). The second missense mutation described is p.His507Arg (H507R) and it also results in a reduced REP1 expression (14). Both mutations were predicted to destabilise the 3D REP1 structure.

We have identified a novel missense variant p.Leu457Pro (L457P), associated with choroideremia. This variant was recently reported along with three other missense alterations following phenotype-genotype analysis of a large choroideremia dataset (12). These four variants, however, were not studied at the protein or functional level, thus their pathogenicity is yet to be determined. We report here the thorough characterisation of the L457P mutation. We studied the RNA expression levels, REP1 protein levels, and the prenylation status of patient fibroblasts. Furthermore, we generated L457P-patient-specific induced pluripotent stem cell (iPSc)-derived RPE and confirmed the results in the cell type affected by the disease. Taken together, these results allowed us to definitively identify the third pathogenic missense mutation associated with choroideremia. Lastly, considering the current climate of gene therapy for choroideremia, for the first time, we assayed whether the presence of a mutated REP1 protein could potentially be a hindrance for a gene replacement strategy by testing for the restoration of prenylation in the patient-specific iPSc-derived RPE following AAV-mediated gene transfer. These results are important when considering inclusion into a clinical gene therapy trial.

Results

Clinical phenotype

The family of the proband, referred to as CHM6 in this study, included three living affected males born from three female carriers

(Fig. 1A). The proband, patient III:9, was examined at 37 years of age. He noted night blindness at 7 years of age and had difficulties in mobility at 30 years. He had no reading impairment. His best-corrected visual acuity was 20/20 in both eyes with $-1.25 \times -4.75 \times 65$ degrees and $-1.00 \times -3.50 \times 105$ degrees in the right and left eyes, respectively. Fundus examination showed typical chorioretinal atrophy, with absence of autofluorescence, in the retinal periphery and spots of pigment deposits (Fig. 1B). A narrowed central islet of preserved retina was present in each eye (Fig. 1C). On an optical coherence tomography (OCT) scan, the ellipsoid zone and outer nuclear layer were absent in the regions where the choroid was atrophic. Typical tubulations and interlamellar bridges were noted. The visual field showed a central vision on 10–12 degrees, a large infero-temporal remnant of vision between 50–80 degrees, and a few spots of vision in the superior visual field. The full field electroretinogram (ERG) was virtually not recordable in scotopic conditions. By contrast, photopic responses were measurable but reduced to 15–20% of the normal amplitude.

Patient III:2 was examined at 23 years. He had night blindness since 10 years of age but had no moving or reading difficulties. His visual acuity was 20/20 in each eye with $-0.75 \times -2.00 \times 90$ degrees in the right eye and no correction in the left eye. Fundus examination showed a profile similar to that of patient III:9 with peripheral chorioretinal atrophy (Fig. 1D) and preservation of a rounded central islet of retina, larger than in patient III:9 (Fig. 1E). There was a partial loss of peripheral visual field with a bilateral annular scotoma that extended from 5 to 10 degrees from the central vision to 30–40 degrees in the periphery. The full field ERG was not recordable in scotopic conditions. Photopic responses were measurable but reduced to 20% of the normal amplitude.

We could not directly examine patient III:4. However, we know he was exempted from military duties at 25 years of age for night blindness and also had moving difficulties at this age. At 48 years, he could read only large letters. His visual field showed less than 5 degrees of central vision with a large infero-temporal remnant of vision between 70 and 90 degrees.

In conclusion, the three patients had typical choroideremia with a similar progression with age. Sequence analysis of all the *CHM* exons in the DNA from patients III:9 and III:2 resulted in the detection of the segregating missense mutation c.1370T > C in exon 11 that is predicted to result in the protein change L457P.

Effect of the c.1370T > C mutation on expression

We first assayed the effect of the c.1370T > C mutation carried by patient CHM6 at the RNA level by quantitative reverse transcription (RT) PCR (qPCR) analysis. This was compared to the expression in WT fibroblasts and in fibroblasts from a CHM patient who carries a deletion of exon 8 (previously referred to as CHM1 (10)). In the fibroblasts from patient CHM1, the *CHM* transcript was detectable at a level that was approximately equivalent to 20% of wild type levels (Fig. 2A). Conversely, the *CHM* transcript in the CHM6 fibroblasts was detectable at levels similar to WT. At the protein level, the deletion of exon 8 in patient CHM1 gives rise to a frameshift and premature protein truncation (10). Consistently, no REP1 could be detected by western blot analysis (Fig. 2B). In comparison, the translated protein carrying the L457P missense mutation, is detectable by western blot analysis but at a level equivalent to ~14% of WT.

Thus, the missense mutation c.1370T > C results in the expression of stable *CHM* transcript but a reduced expression of mutant REP1 protein.

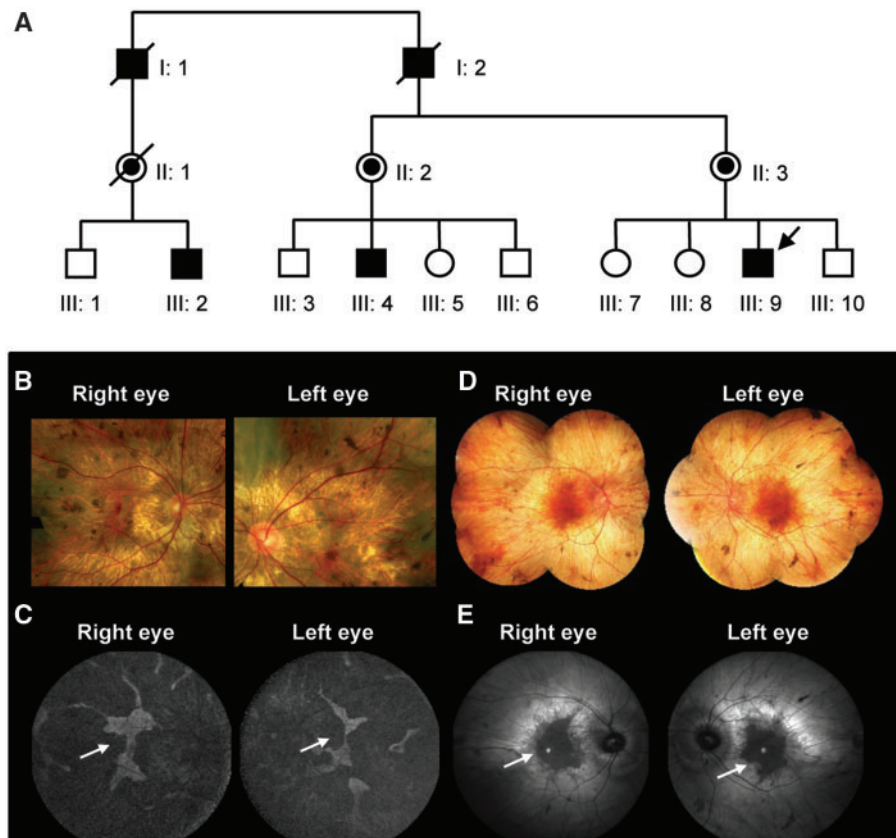


Figure 1. Clinical data of the patients from the family CHM6. (A) Pedigree of the family CHM6. Males affected with choroideremia are indicated by filled symbols, carrier females by symbols with a dark dot, and unaffected individuals by open symbols. Arrow indicates the proband. Clinical data of patient III:9: (B) Fundus photographs show the chorioretinal atrophy in the posterior pole with pigment deposits; (C) Fundus autofluorescence imaging reveals the narrow central islet of the preserved retina (arrows), which appears white while the peripheral retina is dark by absence of autofluorescence. Clinical data of patient III:2: (D) Wide-field fundus photography show the chorioretinal atrophy of the whole fundus except for the central islet of preserved retina coloured in red; (E) Infrared fundus imaging reveals the dark round-shaped central islet of the preserved retina (arrows).

Effect of the L457P missense mutation on function

We then assayed for the effect of the L457P mutation on REP1 function using an *in vitro* prenylation assay. In this assay, unprenylated Rab GTPases present in the cytosol are available for *in vitro* prenylation using a biotinylated prenyl donor. Subsequent detection of biotinylated Rabs by western blot analysis provides a semi-quantitative analysis of the amount of unprenylated Rabs originally present in the cytosol (10). We previously showed that fibroblasts from CHM patients carrying loss-of-function mutations had unprenylated Rab GTPase levels that were between 4- and 10-fold higher than wild type (15). Here, we performed *in vitro* prenylation assays in CHM6 fibroblasts (one representative assay is shown in Fig. 2C). The biotinylated Rab population is barely detectable in wild type fibroblasts as, due to the presence of functional REP proteins, most Rabs are associated with vesicular membranes and hence not available for *in vitro* prenylation. By contrast, the biotinylated Rab population is clearly visible in fibroblasts from patient CHM6. A semi-quantification of the biotinylated Rab signal normalised to the β -actin loading control from three independent assays, indicates that the original unprenylated Rab pool in CHM6 fibroblasts is ~6-fold higher than that observed in control cells (Fig. 2D).

Thus, the missense mutation L457P results in the same biochemical defect as loss-of-function CHM mutations, i.e. an underprenylation of Rab GTPases (10,15).

Generation of control and patient iPSc

To generate a pertinent model for further studies of the L457P mutation, we reprogrammed control fibroblasts and fibroblasts from patient CHM6 into induced pluripotent stem cells (iPSc) using episomal Sendai virus vectors carrying the Yamanaka transcription factor cocktail. We assayed the iPSc from P10 for pluripotency by testing for the persistence of exogenous gene expression from the Sendai vectors (Fig. 3A) and the expression of endogenous host genes (Fig. 3B–D). As a positive control, the expression of the transgenes could be detected in transduced control and patient fibroblasts 7-days post-reprogramming (Fig. 3A). No expression could be detected in non-transduced fibroblasts. Similarly, no expression was detected in the reprogrammed control and patient iPSc, demonstrating the loss of the episomal reprogramming vectors. By contrast, the endogenous host pluripotency genes *LIN28A* (Fig. 3B), *NANOG* (Fig. 3C) and *OCT3/4* (Fig. 3D) were expressed in the iPSc confirming pluripotency. We also assayed the genotype of the wild type and patient iPSc by sequence analysis of exon 11. In the DNA from wild type iPSc, we detected a T at the position corresponding to c.1370 in the CHM open reading frame (Fig. 3E). In contrast, in the DNA from the iPSc of patient CHM6, a C replaced the T at the same position (Fig. 3F), correlating with the CTG to CCG codon change that gives rise to the predicted leucine to proline substitution. Lastly, we assayed the generated control and patient iPSc (P13 and P10, respectively) for genetic stability. No

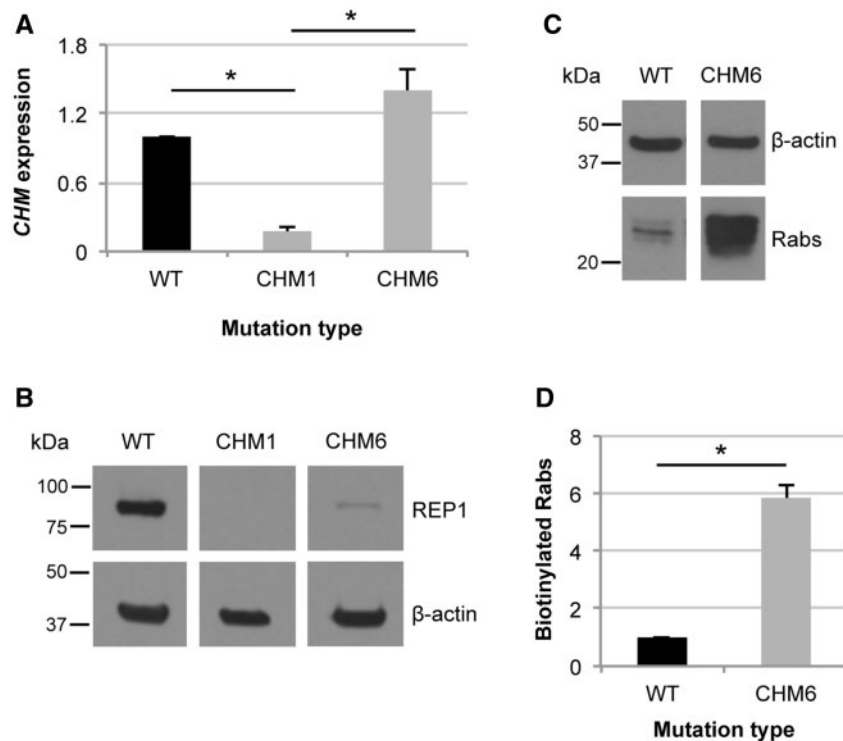


Figure 2. Effect of the missense mutation in patient fibroblasts. (A) qPCR analysis of *CHM* expression (in relative units) shows that the c.1370T > C mutation in CHM6 fibroblasts results in mRNA expression levels that are similar to wild type (WT) cells. This is in comparison to CHM1 fibroblasts, which carry a deletion of exon 8, and show significantly decreased *CHM* transcript levels (data expressed as mean \pm SEM, $n = 3$; $P < 0.05$). (B) Western blot analysis shows that the L457P REP1 protein has a size equivalent to the wild type REP1 protein but with reduced expression. (C) A representative *in vitro* prenylation assay using a biotinylated prenyl donor followed by western blot analysis shows a weak signal of incorporated biotin for the wild type (WT) fibroblasts as compared to the intense signal for CHM6. (D) Semi-quantification of the biotinylated Rab pool (in relative units), after normalisation with β -actin loading, confirms a significant accumulation of unprenylated Rabs in the cells of patient CHM6 as compared to wild type (data expressed as mean \pm SEM, $n = 3$; $P < 0.05$).

large rearrangements could be detected by karyotype analysis for wild type (Fig. 3G) or CHM6 (Fig. 3H) iPSc.

Taken together, the CHM6 patient-derived iPSc are pluripotent, genetically stable and carry the c.1370T > C mutation, and are hence suitable for differentiation into retinal pigment epithelium (RPE).

Generation of control and patient iPSc-derived RPE

We differentiated the wild type and CHM6 iPSc (Fig. 4A) into RPE using a spontaneous differentiation protocol (10). The differentiation process resulted in the appearance of pigmented foci (Fig. 4B), which, when dissected and passaged onto Matrigel-coated dishes, displayed a characteristic cobblestone monolayer composed of tightly packed, polygonal, pigmented cells (Fig. 4C). Transmission electron microscopy (TEM) confirmed a polarised epithelial monolayer for control (data not shown) and CHM6 iPSc-derived RPE comprising apical microvilli, a basal nucleus and pigmented melanosomes (Fig. 4D) as well as apical tight junctions (Fig. 4E). Transepithelial resistance (TER) measurements were taken weekly and the epithelia were confirmed as tight from 4 weeks post-passaging (Fig. 4F), consistent with TEM observations, when the TER values exceeded $150 \Omega/\text{cm}^2$ (16). Typical RPE genes, such as *RDH5*, *MERTK*, *ZO-1*, *TYR*, *BEST1*, *RLBP1* and *PAX6*, were also expressed at the same stage (Fig. 4G). Immunofluorescence (IF) studies showed the presence of the RPE-characteristic markers CRALBP and ZO-1 (Fig. 4H), and LRAT and Bestrophin-1 (Fig. 4I) in control (data not shown) and patient iPSc-derived RPE. Orthogonal visualization and 3D

reconstruction confirmed the polarization of the epithelium, showing an apical localisation of ZO-1 (Fig. 4H in red), a cytosolic localisation for CRALBP (Fig. 4H in green), a perinuclear localisation of LRAT (Fig. 4I in red) and, lastly, a lateral localisation for Bestrophin-1 (Fig. 4I in green).

Taken together, we generated a characteristic iPSc-derived RPE monolayer for the patient CHM6.

AAV-mediated gene transfer studies

We previously showed that the iPSc-derived RPE is a powerful tool for retinal gene transfer studies (10). In that study, we performed AAV2/5-mediated gene transfer of the *CHM* gene into iPSc-derived RPE from patient CHM1 and we restored the prenylation status of Rab GTPases to wild type levels. Here, we tested the ability of an exogenous REP1 protein to restore prenylation in the presence of a mutated REP1 protein.

Firstly, to confirm that the generated tissue was amenable to transduction, we performed a comparative transduction study using an AAV2/5 vector expressing EGFP of the iPSc-derived RPE from patient CHM6 in comparison to that of patient CHM1. The AAV2/5-CAG-EGFP vector readily transduced both tissues although slightly superior transduction efficiency was observed for CHM1, as determined by FACS (1.5-fold higher; Fig. 5A) and western blot (1.8-fold higher; Fig. 5B) analyses, compared to CHM6. EGFP expression in the iPSc-derived RPE could be detected by IF studies (Fig. 5C). We then transduced both CHM1 and CHM6 RPE with an AAV2/5 vector carrying *CHM* under control of the CAG promoter. In non-transduced RPE, REP1

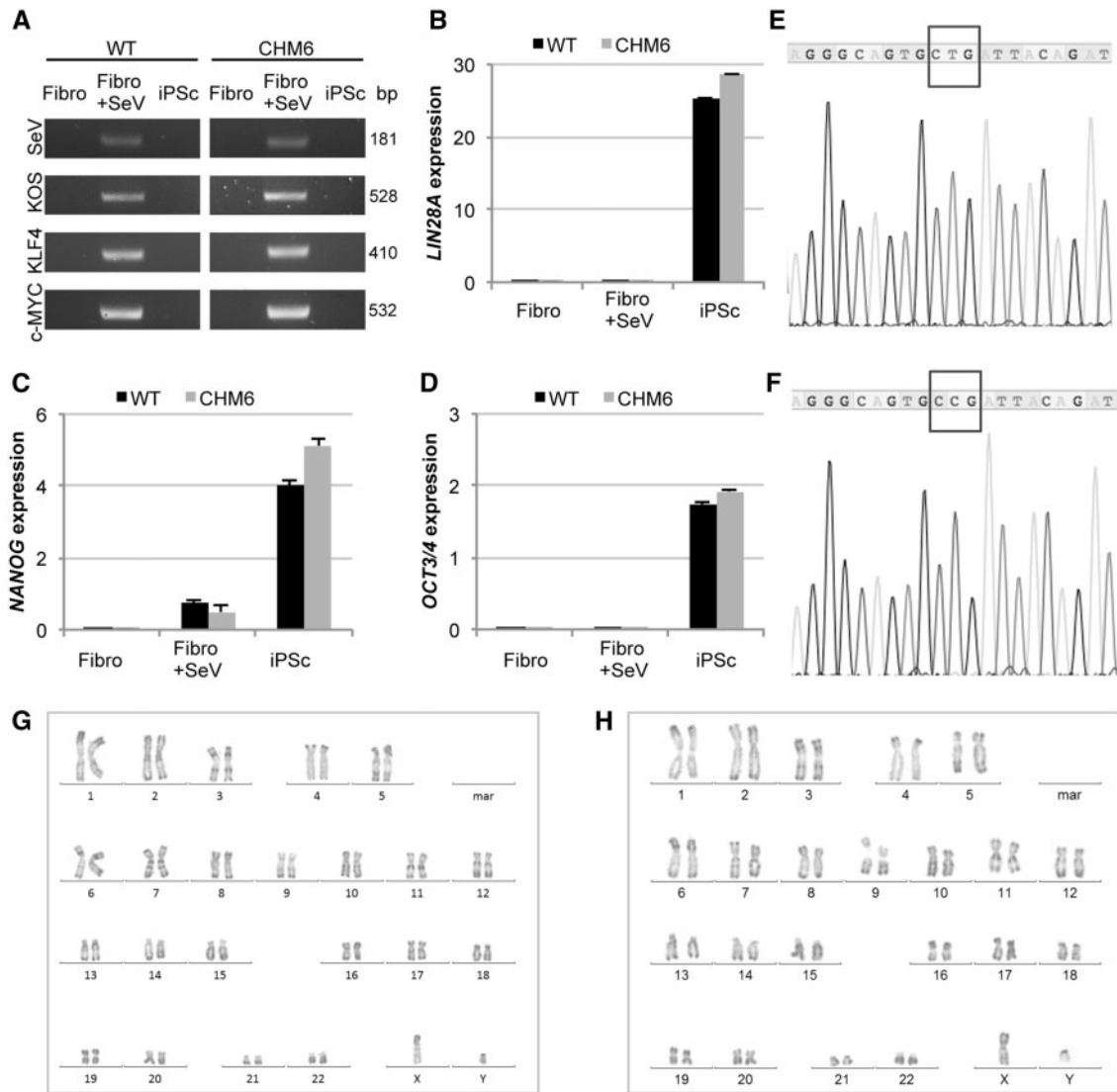


Figure 3. Quality control of wild type and CHM6 iPSc. (A) RT-PCR analysis using primers specific to the Sendai virus vector backbone (SeV), the reprogramming vector carrying the KLF4, OCT3/4 and SOX2 polycistronic cassette (KOS), the vector carrying the KLF4 transgene (KLF4), and the Sendai vector carrying the c-MYC transgene (c-MYC) shows that the episomal vectors are no longer present in the wild type and CHM6 iPSc. Negative control, non-transduced fibroblasts (Fibro). Positive control, SeV-transduced-fibroblasts collected 7 days post-transduction (Fibro +SeV). qPCR analysis of endogenous LIN28A (B), NANOG (C) and OCT3/4 (D) expression shows an increased expression of the host pluripotency genes (in relative units) in the wild type (black bars) and CHM6 (grey bars) iPSc as compared to non-transduced (Fibro) and transduced (Fibro +SeV) fibroblasts. (E) Sequence analysis of the genomic DNA of the wild type iPSc showing a T at position c.1370 (boxed area spans c.1369-1671). (F) Sequence analysis of the genomic DNA of the CHM6 sequence showing the T > C transition at position c.1370. Karyotype analysis of the wild type (G) and CHM6 (H) iPSc did not detect large chromosomal rearrangements.

expression could not be detected for either CHM1 or CHM6 (Fig. 5D) by IF studies; the level of endogenous REP1 expression per cell in the CHM6 RPE was likely too low to be detected by the antibody. The outline of the cobblestoned RPE is readily visible following co-labelling of the apical tight junction marker ZO-1. By contrast, following transduction with AAV2/5-CAG-CHM and overexpression, REP1 was readily detectable by IF studies in both CHM1 and CHM6 iPSc-derived RPE.

In parallel, we assayed REP1 expression in the non-transduced and transduced RPE by western blot analysis. Interestingly, following hybridisation with a monoclonal anti-REP1 antibody, we strongly detected two REP1-specific bands in the control iPSc-derived RPE (Fig. 6A). The first band had a size of ~90 kDa and the second of ~35 kDa; we also detected a non-specific band of ~80 kDa that was present in all wells. This profile was either not

detected, or faintly detected, in fibroblasts and iPSc (data not shown). However, in both these other cell types the 90-kDa band was the most predominant, in contrast to the situation in the RPE. Consistent with our results in the patient fibroblasts, REP1 was not detected in the RPE of patient CHM1 whereas a faint expression was detected in patient CHM6 (Fig. 6A). Semi quantification of the blot indicated that expression of the ~90-kDa REP1 band in patient CHM6 was equivalent to ~10% of wild type (Fig. 6B); the expression profile of the ~35-kDa band mimicked that of the larger band. Upon transduction with AAV2/5-CAG-CHM, we observed the appearance of the same two REP1 bands (Fig. 6A) with a stronger expression in the RPE of patient CHM1 (140% of wild type) as compared to patient CHM6 (55% of wild type; Fig. 6B). This correlated with the superior CHM1 transduction efficiency observed following transduction with AAV2/5-CAG-EGFP.

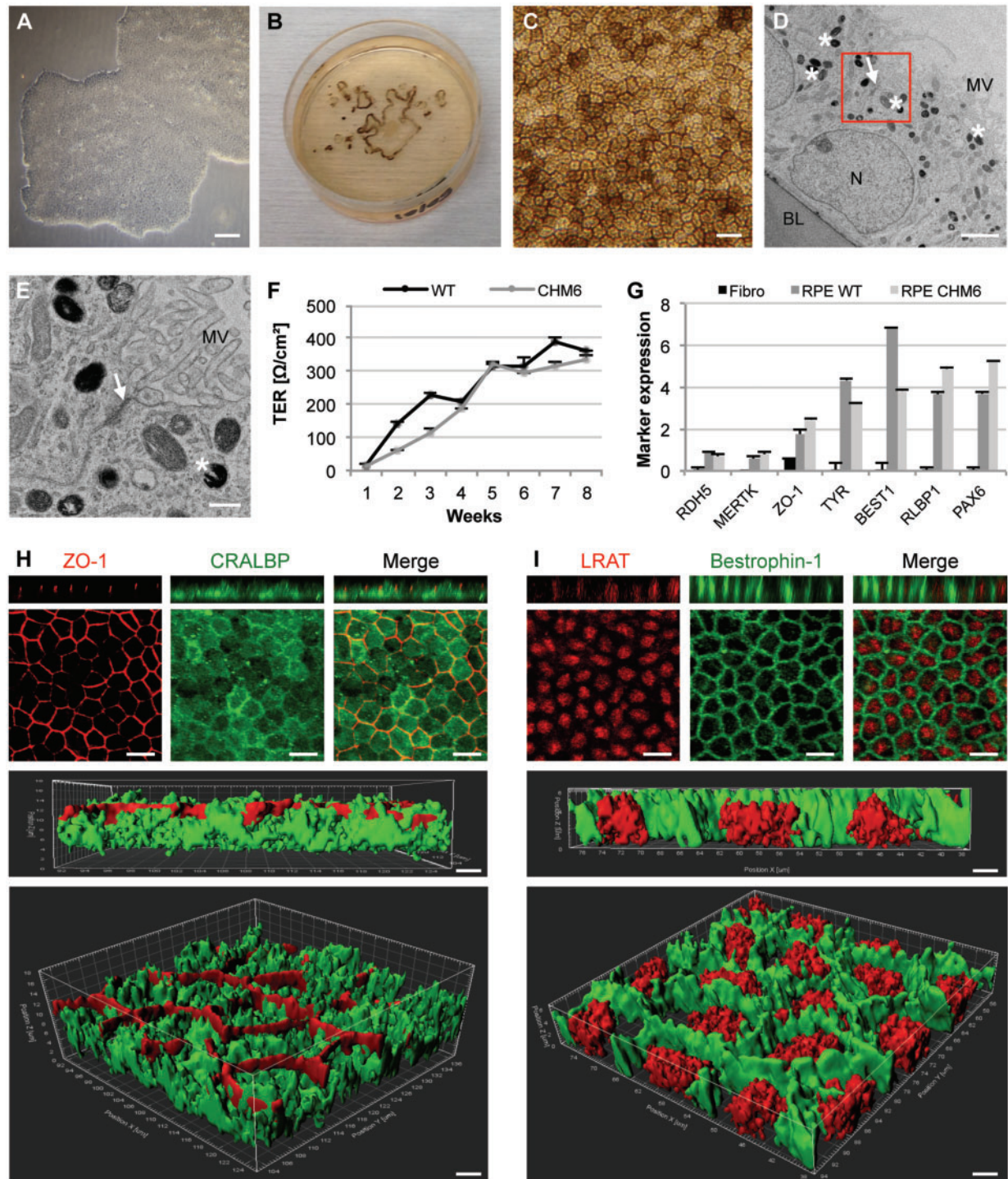


Figure 4. Generation and characterisation of patient CHM6 iPSc-derived RPE. (A) iPSc colonies cultured under feeder-free conditions. Scale bar = 200 μm . (B) Pigmented foci appearing in iPSc plates (35 mm) during the spontaneous differentiation process. (C) Pigmented, cobblestoned iPSc-derived RPE monolayer. Scale bar = 20 μm . (D) TEM analysis shows the iPSc-derived monolayer as a polarized epithelium with microvilli (MV) on the apical side, apical tight junctions (arrow), melanosomes (asterisks) distributed throughout the apical cytosol, a nucleus (N) on the basal side, and a basal lamina (BL) between the epithelium and the filter. Scale bar = 2 μm . (E) TEM at higher magnification (red square in panel 4D) to highlight the tight junction (arrow), melanosomes (asterisks) and the microvilli (MV). Scale bar = 500 nm. (F) TER of wild type (black line) and CHM6 (grey line) iPSc-derived RPE was measured each week after P3 seeding and presented as normalized Ω/cm^2 (data expressed as mean \pm SEM, $n = 3$). (G) qPCR analysis shows an increased expression (in relative units) of the typical RPE markers RDH5, MERTK, ZO-1, TYR, BEST1, RLBP1 and PAX6 in wild type (dark grey bars) and CHM6 iPSc-derived RPE (light grey bars) as compared with fibroblasts (black bars) (data expressed as mean \pm SEM, $n = 3$). (H) IF studies of the iPSc-derived RPE monolayer followed by confocal analysis, demonstrate the expression of ZO-1 (red) and CRALBP (green). Scale bars = 15 μm . The orthogonal visualization (upper panels) and the 3D reconstruction (lower panels; scale bars = 2 μm) show the apical localization of ZO-1 and the cytosolic localization of CRALBP. (I) IF studies of the iPSc-derived RPE monolayer followed by confocal analysis, demonstrate the expression of LRAT (red) and Bestrophin-1 (green). Scale bars = 15 μm . The orthogonal visualization and the 3D reconstruction (scale bars = 2 μm) show the perinuclear localization of LRAT (red) and the expression of Bestrophin-1 (green) along the lateral membrane of the iPSc-derived RPE.

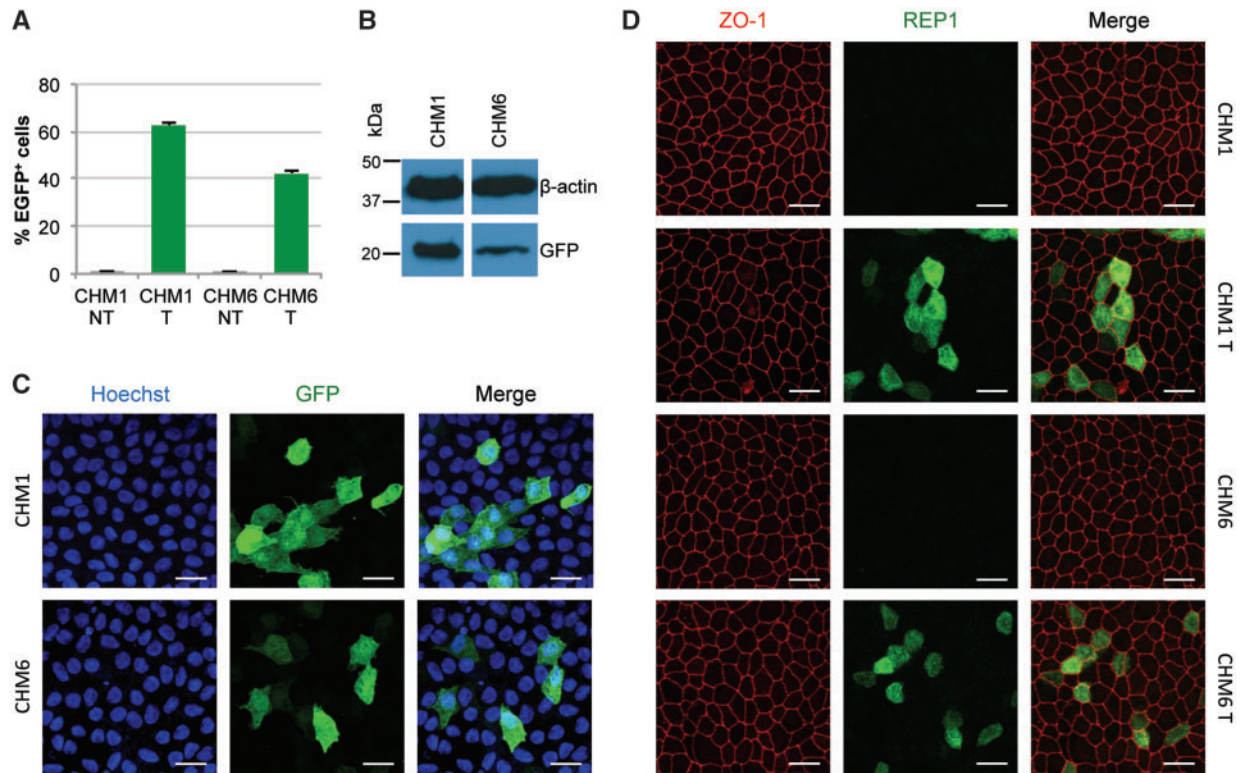


Figure 5. Transduction of wild type and patient iPSc-derived RPE. (A) FACS analysis following transduction with an AAV2/5-CAG-EGFP vector shows a transduction efficiency of ~60% for CHM1 (CHM1 T) and ~40% for CHM6 (CHM6 T) iPSc-derived RPE (expressed as percentage of EGFP-positive cells). No EGFP-positive cells could be detected in non-transduced CHM1 (CHM1 NT) or CHM6 (CHM6 NT) samples. (B) Western blot analysis confirms the higher transduction efficiency for CHM1 as compared to CHM6. (C) Immunofluorescence studies showing EGFP expression following transduction of CHM1 and CHM6 iPSc-derived RPE with AAV2/5-CAG-EGFP (in green). Nuclei are labelled in blue. (D) Immunofluorescence studies showing REP1 expression following transduction of CHM1 (CHM1 T) and CHM6 (CHM6 T) iPSc-derived RPE by AAV2/5-CAG-CHM (in green). The contours of the RPE cells are immunolabelled by an anti-ZO-1 antibody, in red. Endogenous REP1 cannot be detected in either non-transduced CHM1 or CHM6 RPE. Scale bars = 20 μ m.

Finally, we assayed for a functional restoration post-transduction using *in vitro* prenylation assays. One representative assay is shown in Figure 6C, where low levels of biotinylated Rabs are detected in wild-type cells as was the case in fibroblasts. By contrast, in non-transduced CHM1 and CHM6 cells, due to the absence of functional REP1, the amount of biotinylated Rab proteins is higher than in control cells (Fig. 6C). A semi-quantification following normalisation to β -actin levels of three independent experiments is presented in Figure 6D. Three-weeks post-treatment with the AAV2/5-CAG-CHM vector, we noted a decrease in unprenylated Rab levels for both CHM1 and CHM6, which was coherent with the appearance of a detectable REP1 expression in the cytosol (Fig. 5D). Unprenylated Rab levels were decreased by almost half in both patients and were significantly decreased for CHM6 ($P < 0.05$; Fig. 5D).

Taken together, AAV2/5-mediated transduction of CHM6 iPSc-derived RPE results in a significant reduction of the unprenylated Rab population, despite the presence of a mutated REP1 protein.

Discussion

Choroideremia is an X-linked disease due to mutations in the CHM gene encoding Rab Escort Protein 1 (REP1). REP1 is a ubiquitous chaperone protein allowing the correct prenylation of Rab GTPases and their subsequent delivery to their membrane targets (17). This prenylation process requires the binding of REP1 to the Rab GTPases in order to present them to the enzyme Rab

GeranylGeranyl Transferase II (RGGTase II) that will add the lipid prenyl donor. Subsequently, REP1 chaperones the prenylated proteins to their final target. It is not yet known how this underlying biochemical defect gives rise to the clinical signs associated with the disease. Generally, affected males experience an onset of night blindness in their first decade of life (7). Progressive peripheral visual field loss begins in the second decade and the peripheral field is highly constricted by the fourth to fifth decade. The pathogenic mutations associated with choroideremia have been extensively published, but to date there has been no evidence of any phenotype-genotype correlations (12,15). Interestingly, the majority of CHM mutations are loss of function mutations. Missense variants have been rarely described (12–15,18) and of these, only two, L550P (13) and H507R (14) have been shown to have an impact on protein production.

The effect of the first causative missense variant, L550P, was not studied at the RNA level but it was shown by western blot analysis that a protein product could be faintly detected in patient fibroblasts. Interestingly, no protein was detected in patient PBMCs, which could suggest a differential expression of REP1 with regards to tissue. Consistent with the reduced REP1 expression, modelling studies predicted that the L550P mutation affected the stability of the REP1 β -sheet and, in turn, the integrity of the whole molecule (13). The expression of the second causative missense variant, H507R, was analysed by RT-PCR studies and did not impair RNA production. Western blot analyses of patient lymphocytes detected a low level of mutant protein. Lastly, the H507R mutation was predicted to destabilise

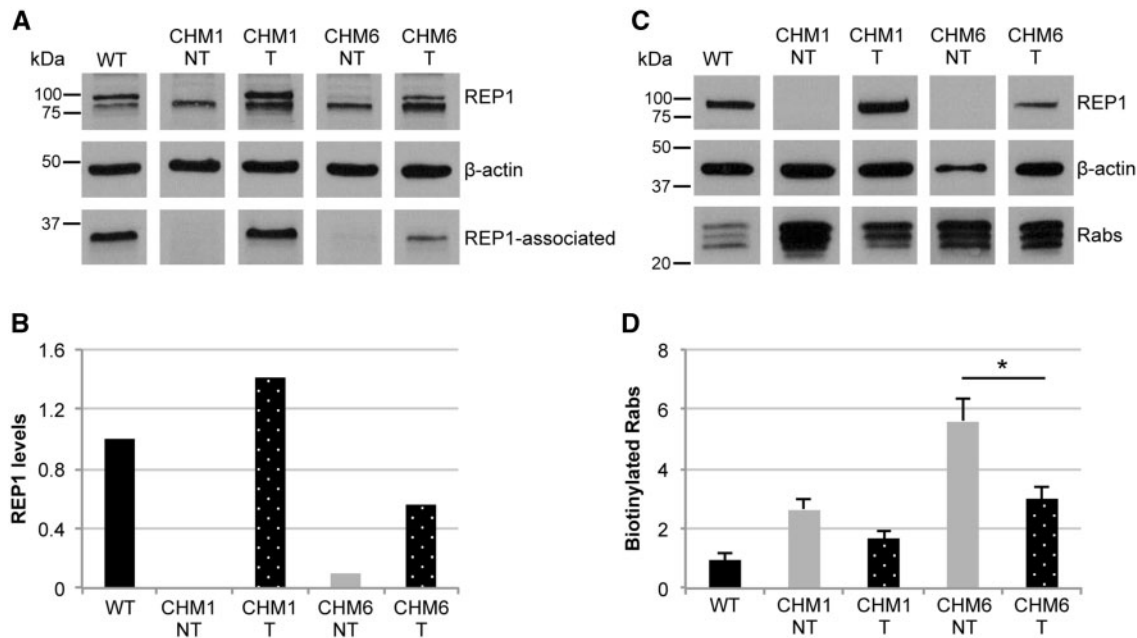


Figure 6. Effect of exogenous REP1 expression on unprenylated Rab GTPases. (A) Western blot analysis of REP1 expression in wild type (WT), non-transduced CHM1 (CHM1 NT) and non-transduced CHM6 (CHM6 NT) iPSc-derived RPE, and in CHM1 (CHM1 T) and CHM6 (CHM6 T) RPE transduced with 100 000 vg/cell of AAV2/5-CAG-CHM. An ~90-kDa band corresponding to REP1 can be readily seen in the wild type and in transduced cells from patients CHM1 and CHM6. REP1 expression is not detectable in non-transduced CHM1 RPE. A faint band can be seen in non-transduced CHM6 RPE, consistent with observations in fibroblasts. A non-specific ~80-kDa band is detected in all lanes. An additional ~35-kDa band appears concomitantly to the ~90-kDa REP1 band in all lanes with the exception of non-transduced CHM1. (B) Quantification of the expression (in relative units) of the ~90-kDa REP1 band in panel A, following normalisation to β-actin levels, confirms the low level of expression of REP1 in non-transduced CHM6 RPE, and the higher efficacy of transduction in CHM1 RPE compared to CHM6. (C) A representative *in vitro* prenylation assay followed by western blot analysis of incorporated biotinylated prenyl donor in wild type (WT), non-transduced CHM1 (CHM1 NT), non-transduced CHM6 (CHM6 NT) RPE and in CHM1 (CHM1 T) and CHM6 (CHM6 T) RPE transduced with 100 000 vg/cell of AAV2/5-CAG-CHM. The expression of REP1 can be seen in the wild type and transduced cells. (D) Normalisation to β-actin loading levels and semi-quantification indicates that the biotinylated Rab content (in relative units) in transduced CHM6 RPE is significantly lower (asterisk; $P < 0.05$) than that of non-transduced CHM6 RPE (data expressed as mean \pm SEM, $n = 3$).

REP1 protein structure, and co-immunoprecipitation studies showed that it affected the ability of REP1 to interact with RGGTase (14).

Using both RNA and protein expression, and functional assays, we were able to confirm the pathogenicity of a third missense mutation, L457P, associated with choroideremia. Similar to the H507R mutation, by qPCR analysis, we showed that L457P results in wild type levels of *CHM* transcript production. By contrast, using western blot analysis of patient skin fibroblasts, we showed that protein expression was severely reduced as compared to wild type expression. We have previously shown that the levels of unprenylated Rab GTPases were higher (4- to 10-fold) in the fibroblasts of *CHM* patients carrying loss of function mutations with no detectable REP1 protein as compared to wild type cells (15). We assayed the prenylation status of the fibroblasts of patient CHM6 carrying the L457P mutation and we showed that the levels of unprenylated Rab GTPases were ~6-fold higher than in wild-type fibroblasts, thus in the range observed for loss-of-function mutations. Taken together, these data showed that the missense L457P variant is indeed pathogenic and joins the short list of missense *CHM* mutations identified to date.

The paucity of missense mutations associated with choroideremia is intriguing and raises certain questions. Firstly, could a mutant REP1 protein interfere with the residual prenylation pathway in patient cells conducted by REP2, thus exacerbating the phenotype? The clinical phenotype observed in our patients is on the average what is found in choroideremia (19), thus arguing against this. In all three patients, night blindness was

noted in late infancy or adolescence, visual field impairment in young adulthood and visual acuity was virtually normal until 40 years of age. The eldest patient is now aged 56 years and uses a white cane for mobility. Therefore, this mutation leads to pathogenic consequences with an apparently similar progression in the three patients and an average severity.

Secondly, considering the current climate of choroideremia gene therapy, could the presence of a mutated REP1 protein have a negative effect on exogenous wild-type REP1 expression? We previously showed that patient-specific iPSc-derived RPE is an excellent model for gene transfer studies of choroideremia (10). In an iPSc-derived RPE model from patient CHM1 carrying a loss-of-function mutation, we were able to provide a proof-of-concept for the correction of the prenylation defect using AAV2/5-mediated gene delivery of *CHM*. Using a similar approach, we generated an iPSc-derived RPE model from fibroblasts of patient CHM6 carrying the L457P mutation and assayed the effect of this mutation on exogenous gene transfer.

For comparative purposes, we conducted gene transfer studies in parallel on iPSc-derived RPE from patient CHM6 and from patient CHM1. Western blot analyses of wild type and patient iPSc-derived RPE both before and after transduction, revealed a differential expression, excluding that of the ~90 kDa REP1 protein, in this tissue as compared to that of fibroblasts and iPSc. Firstly, an ~80 kDa band was detected in all wells independently of REP1 expression. This band was not detected in the *in vitro* prenylation assay that was performed exclusively on the cytosolic cell fraction, suggesting that the antibody may cross-react with an extra-cytosolic protein (such as a nuclear or membrane

protein). Secondly, an additional ~35-kDa REP1-associated protein was highly expressed in RPE whereas it was only weakly detectable in other cell types. Moreover, this smaller band was present in the control RPE, and in the CHM1 and CHM6 RPE after transduction with the AAV2/5 expressing CHM. It was not detected in the CHM1 RPE prior to transduction, consistent with the absence of REP1, and very faintly in the CHM6 RPE, consistent with the faint detection of REP1. Thus taken together, the ~35-kDa protein is tightly associated with REP1 expression whether it is endogenous or exogenous.

There are three isoforms of CHM that can be found in the NCBI gene database. The first encodes the 653 aa REP1 protein, NP_000381.1, which migrates at ~90 kDa. The second, NP_001138886.1, is predicted to encode a 110 aa protein that matches with the first N-terminal 105 aa residues of REP1. We do not think that this corresponds to the ~35 kDa protein detected by western blot analysis because 1) the predicted size (~12 kDa) is smaller and 2) the epitope of the anti-REP1 antibody (2F1) used is predicted to be situated within the C-terminal 451 aa of the protein (20) and therefore would not bind this isoform. The third isoform, NP_001307888, arises due to the presence of an alternative exon 1 and is predicted to encode a 505 aa protein, which starts at the methionine residue situated at position 149 of REP1. Therefore, as it comprises the C-terminal region, the 2F1 antibody could theoretically detect it. However, the predicted size (~56 kDa) of this isoform is larger than that detected.

Thus, as the detected ~35 kDa band does not appear to correspond to any of the reported CHM isoforms, and as an alternative isoform could not explain the presence of this protein in transduced wells into which only the CHM cDNA was introduced, we performed a bioinformatics analysis of REP1 for evidence of proteolytic processing. A putative Caspase I cleavage was exclusively predicted at position 467 aa. This would result in an N-terminal fragment of 51 kDa and a C-terminal fragment of 20 kDa, which does not correspond to the detected size. Although other sites were not predicted, proteolytic cleavage still remains a possibility but this may only be resolved following protein sequencing of this additional band detected by the anti-REP1 antibody. Nonetheless, this differential RPE expression is intriguing when considering that it is mainly the retina that is clinically affected by REP1 mutations, raising the question of an additional specific role.

In vitro prenylation studies of the L457P iPSc-derived RPE showed that unprenylated Rab levels were on average 5.5-fold higher than control RPE, consistent with our observations on the corresponding fibroblasts. Following gene transfer with the AAV2/5 vector expressing CHM, we reduced unprenylated Rab levels to levels that were ~3-fold higher than wild type. Levels were not normalised following gene transfer, but this 45% reduction correlated with the observed transduction efficiency of ~40% using the AAV2/5 vector expressing EGFP. Previously, we showed that the CHM1 iPSc-derived RPE contained unprenylated Rab levels that were ~4-fold higher than wild type and that were normalised post-transduction (10). Here, the levels of unprenylated Rabs in the CHM1 RPE were on average 3-fold higher than wild type. We do observe modest variations between batches of iPSc-derived RPE and this likely depends on the differentiation and the age of the cells post-differentiation. Following gene transfer, we reduced unprenylated Rab levels to levels that were ~1.5-fold higher than wild type. This 50% reduction was compatible with the observed transduction efficiency of ~60% for the CHM1 iPSc-derived RPE using the AAV2/5-EGFP vector. Thus taken together, the CHM1 iPSc-derived RPE showed slightly higher transduction efficiency than that of

CHM6, which correlated with a greater reduction in unprenylated Rab levels.

We have previously shown that the prenylation status of cells can be variable even when obtained from siblings carrying the same mutation (15). This could be inherent to the cells or due to uncontrollable technical parameters associated with their culture. As a consequence, we do not wish to put too much emphasis on the observation that the cells from patient CHM6 carrying the L457P mutation showed higher unprenylated Rab levels than the cells from patient CHM1 carrying the loss-of-function mutation. In contrast, we can emphasise that we reduced unprenylated Rab levels in both cell types to a similar level, if we take into account transduction efficiency differences. This indicates that the L457P mutation did not hinder the function of the exogenous REP1 protein. Thus, CHM patients carrying missense mutations that allow a residual mutated protein expression could still be candidates for future clinical trials. In conclusion, this study highlights the predictive value of patient-specific iPSc-derived RPE for determining the pathogenicity of novel variants and for therapy screening prior to inclusion in clinical trials.

Materials and Methods

Clinical investigations and mutation detection

Patients underwent standard ophthalmologic examinations (refraction, visual acuity, slit-lamp examination, applanation tonometry and funduscopy). Kinetic visual fields were determined with a Goldmann perimeter with targets V4e, III4e and I4e. OCT measurement of the macula was performed using a spectral-domain optical coherence tomography (Spectralis, Heidelberg, Germany). Autofluorescence measurements were obtained with the Heidelberg retina angiograph 2 (Heidelberg Engineering, Dossenheim, Germany) and fundus pictures were taken. Full-field ERGs were recorded using a Ganzfeld stimulator (Metrovision, Pérenchies, France) with a bipolar contact lens electrode after maximum dilation of the pupil, according to the International Society for Clinical Electrophysiology of Vision (ISCEV)-standard protocol. Best-corrected visual acuity was measured with Snellen charts in decimal numbers. For mutational analysis, genomic DNA was extracted from peripheral blood using standard procedures, and each CHM exon was PCR-amplified and sequenced (conditions and primer sequences available upon request). Exonic sequences were compared to the *Homo sapiens* CHM sequence (GenBank accession number: NM_000390.2). The nomenclature follows the HGVS recommendations with nucleotide +1 corresponding to the A of the ATG initiation codon.

Skin biopsies and fibroblasts of CHM patients

The skin biopsy of CHM6 was performed under sterile conditions at the Centre of Reference for Genetic Sensory Disorders (CHRU Montpellier) following informed consent. Regional and national ethic committees accorded biomedical research approval under the authorisation number 2014-A00549-38. The corresponding fibroblasts were cultured in AmnioMAX C100 basal medium supplemented with 10% decomplexed FCS (Lonza, Verviers, Belgium), 1% GlutaMAX (Gibco, ThermoFisher Scientific, Villebon sur Yvette, France), 1% penicillin-streptomycin-amphotericin B (Lonza) and 2% AmnioMax-C100 supplement (Gibco) at 37 °C under 5% CO₂.

Generation of iPSc

On day 2, wild type BJ fibroblasts (ATCC CRL2522; kindly provided by Dr J. De Vos, IRMB, Montpellier) and fibroblasts from patient CHM6 were seeded at a density of 1×10^5 cells per 9.4 cm^2 in high glucose DMEM containing GlutaMAX (Gibco) and supplemented with 10% FBS (Gibco), 1% non-essential amino acids (Gibco) and 55 mM β -mercaptoethanol (Gibco). On day 0, cells were reprogrammed using the CytoTune-iPS 2.0 Sendai reprogramming kit (Life Technologies, ThermoFisher Scientific) containing three Sendai virus-based reprogramming vectors (CytoTune 2.0-KOS, -hc-MYC, -hKLF4) expressing KLF4, OCT4, SOX2, and/or c-MYC, according to the manufacturer's recommendations. The medium was refreshed daily until day 7 when the transduced fibroblasts were passed onto dishes coated with 1/100 dilution Corning Matrigel hESC-qualified matrix (Dominique Dutscher, Brumath, France) at a density of 1.25×10^5 cells per 9.4 cm^2 . On day 8, the media was changed to TeSR-E7 Basal Medium (Stemcell Technologies, Grenoble, France). From day 13, emerging iPSc were mechanically passaged using a scalpel under a Lynx stereomicroscope (Vision Engineering SA, Le Plessis Pâté, France) and cultured in Essential 8 Basal Medium (Gibco). Passages were subsequently performed using Versene solution (0.48 mM; Gibco).

Differentiation into RPE

The iPSc were grown to confluence and the Essential 8 Basal Medium was changed to Knockout DMEM medium (Gibco) supplemented with 20% KO serum replacement (Gibco), 1% GlutaMAX (Gibco), 1% non-essential amino acids (Gibco), 0.1% β -mercaptoethanol (Gibco) and 1% penicillin-streptomycin (Gibco). The medium was renewed three times per week during the spontaneous differentiation period. Pigmented foci were manually dissected, pooled, dissociated with 0.25% trypsin, filtered through a $40 \mu\text{m}$ filter and generally seeded at a density of 3×10^4 cells per 0.32 cm^2 on a 1/30 dilution Corning Matrigel. Subsequent passages were performed in the presence of $10 \mu\text{M}$ StemMACS Y-27632 (Miltenyi Biotech, Paris, France). All analyses were performed on iPSc-derived RPE at P3.

Mutation verification

To verify the presence of the c.1370T > C variant situated in exon 11 in cultured iPSc, genomic DNA was isolated using the DNeasy Blood & Tissue Kit (Qiagen, Les Ulis, France) according to the manufacturer's instructions. A 550-bp product was amplified using the F primer 5'-ACT CCT TTG CTT CAG CTG GG-3' situated in intron 10 and the R primer 5'-GGA GAC GTT GGT CAA AGG GT-3' situated in intron 11, and sequenced using the same F primer. The amplified products were cleaned using an ExoSAP-IT PCR Clean-up Kit (GE Healthcare, Velizy Villacoublay, France) prior to sequencing using the BigDye Terminator Cycle Sequencing Ready Reaction kit V3.1 on an Applied Biosystems 3130xL Genetic Analyser (Applied Biosystems, Foster City, CA).

Karyotype analyses

iPSc were grown to 50% confluence in 8 cm^2 dishes. The medium was supplemented with $0.1 \mu\text{g/ml}$ Nocodazole (Sigma-Aldrich) and incubated 3 h at 37°C . The cells were then dissociated with TrypLE (Gibco) and pelleted at 200 g for 10 min at room temperature. The pellet was gently resuspended in 9 ml of buffered hypotonic solution (Genial Genetics, Excilone, Vicq, France)

and incubated for 20 min at 37°C . The reaction was stopped by the addition of 1 ml of ice cold fixation solution (3 vol. methanol: 1 vol. glacial acetic acid) on ice, prior to centrifugation at 200 g for 10 min at 4°C . After three successive washes, the pellet was resuspended in 500 μl ice-cold fixation solution and stored at -20°C until analysis. Analyses were performed by the Chromostem facility (CHRU Montpellier, France).

Reverse transcription and qPCR studies

RNA was isolated using the QiaShredder and RNeasy mini kits (Qiagen) according to the manufacturer's instructions. The isolated RNA was treated with RNase-Free DNase (Qiagen) and 0.15 to $1 \mu\text{g}$ was reverse transcribed using the Superscript III Reverse Transcriptase kit (Life Technologies). RT-PCR with the primers provided by the manufacturer was used to test for the presence or absence of the Sendai vectors in reprogrammed fibroblasts and iPSc. qPCR with the described CHM primers (10) was used to analyse the expression of endogenous CHM in fibroblasts. qPCR using primers specific for endogenous NANOG, LIN28 and OCT3/4 were used to verify pluripotency in iPSc. qPCR with specific primers for RDH5, MERTK, ZO-1, TYR, BEST1, RLBP1 and PAX6 was used to assess the iPSc-derived RPE. All results were normalised to GAPDH expression and primer sequences are available upon request. Reactions were performed using the LightCycler® 480 SYBR Green I Master mix on a LightCycler® 480 II thermal cycler (Roche). Results were analysed using LightCycler® 480 software and the Microsoft Excel programme. Experiments were performed in triplicate.

Western blot analyses

Cells were scraped into cold PBS containing complete protease inhibitor cocktail tablets (Roche, Meylan, France) and centrifuged at 3000 g for 5 min. The pellet was resuspended in 2x Laemmli's sample buffer (Biorad, Marne La Coquette, France) containing 1/25 dilution of β -mercaptoethanol (Sigma-Aldrich) and Benzozase (Sigma-Aldrich). The samples were heated 5 min at 95°C and loaded onto an AnyKD precast MiniProtean TGX Stain Free gel (Biorad). The separated proteins were electrotransferred using a Trans-Blot® Turbo™ PVDF Transfer Pack and System (Biorad). After blocking for 1 h in 0.5% Tween-PBS in 5% skim milk (blocking solution), membranes were incubated with 1:1000 dilution of monoclonal mouse anti-REP1 antibody (clone 2F1; Millipore, Saint Quentin en Yvelines, France) or 1:2000 dilution of rabbit anti-GFP antibody (Invitrogen-Molecular Probes, Life Technologies), and with 1:10 000 dilution in blocking solution of a mouse anti- β -actin antibody (Sigma Aldrich) overnight at 4°C . After 3 washes in 0.5% Tween-PBS, the membrane was incubated with 1:10 000 dilution of horseradish peroxidase (HRP)-conjugated sheep antibody against mouse (Jackson ImmunoResearch, Interchim, Montluçon), or goat antibody against rabbit (Sigma-Aldrich), whole immunoglobulins. The detection step was performed using the Amersham ECL prime western blotting detection reagent (GE Healthcare).

In vitro AAV transduction

The AAV2/5-CAG-CHM and -EGFP vectors were produced by the Viral Vector Production Facility (Nantes, France), as previously described (10), at the following titres: AAV2/5-CAG-CHM – 1×10^{12} vg/ml and AAV2/5-CAG-EGFP – 2.34×10^{12} vg/ml. For the

transduction experiments, iPSc-derived RPE was seeded in 24-well plates or on glass coverslips coated with 20 µg/ml Corning BioCoat Poly-D-Lysine (ThermoFisher Scientific), 5 µg/ml Corning Laminin and 1/30 dilution of Corning Matrigel. Cells were transduced with 100 000 vg/cell of AAV2/5-CAG-CHM in a minimum volume (300 µl) of supplemented knockout DMEM medium for 6 h to promote vector-cell interaction. The wells were then supplemented with extra media and the media refreshed every 3 to 4 days. Prenylation assays were performed in triplicate at 3-wk post-transduction. To assay for transduction efficiency, iPSc-derived RPE was transduced with 100 000 vg/cell of AAV2/5-CAG-EGFP. At the desired timepoint, cells were dissociated with 0.25% trypsin, fixed in 4% Alfa Aesar Paraformaldehyde (PFA; ThermoFisher Scientific) and the number of EGFP-expressing cells analysed using a BD Accuri C6 Flow Cytometer (BD Biosciences, Le Pont de Claix, France). Experiments were performed in duplicate.

Immunofluorescence studies

For the RPE characterisation studies, iPSc-derived RPE was seeded on Matrigel-coated, translucent BD Falcon cell culture inserts with high density 0.4 µm pores (Dominique Dutscher, Brumath, France) in 24-well plates. Cells were fixed with 4% PFA, blocked in 10% donkey serum (Millipore) and 1% BSA (Sigma-Aldrich) and permeabilised with 0.3% Triton X-100 (Sigma-Aldrich). Primary and secondary antibodies were incubated at room temperature for 1 h prior to mounting in ProLong Diamond Antifade Mountant (Molecular probes, Life Technologies). For the gene transfer studies, cells on coverslips were fixed with 4% PFA, blocked in 10% donkey serum (Millipore) and permeabilised with 0.3% Triton X-100 (Sigma-Aldrich). Primary antibodies were incubated overnight at 4°C and the secondary antibody incubated 45 min at room temperature with 0.2 µg/ml bisBenzimide Hoechst (Sigma-Aldrich) prior to mounting in Dako Fluorescent Mounting Media (Dako France SAS, Les Ulis, France). The primary antibodies were 1:100 dilution rabbit anti-human ZO-1 (Invitrogen, Life technologies), 1:1000 dilution mouse anti-human CRALBP (Agrobio, La Ferté St Aubin, France), 1:250 dilution rabbit anti-human LRAT (Abcam), 1:500 dilution mouse anti-human Bestrophin-1 (Abcam), 1:250 dilution mouse anti-human REP1 (clone 2F1), or 1:200 dilution of rabbit anti-GFP antibody (Invitrogen-Molecular probes). The secondary antibodies were 1:500 dilution donkey anti-rabbit IgG-Alexa Fluor 594 or 488, and donkey anti-mouse IgG-Alexa Fluor 488 (Jackson ImmunoResearch laboratories, Suffolk, UK). Cells were observed using a LSM700 confocal microscope or a Zeiss 5 live duo highspeed/spectral confocal microscope, and image acquisition performed using the corresponding acquisition software (Carl Zeiss SAS; Montpellier RIO Imaging (MRI) facility). Image analysis and 3D reconstruction were performed with the Imaris software (Bitplane, Oxford Instruments, AGAR, Paris, France).

Ultrastructural evaluation

Four-weeks post-passaging, the iPSc-derived RPE-cultured inserts were immersed in a solution of 2.5% glutaraldehyde in PHEM buffer (1X, pH 7.4) overnight at 4°C. They were then rinsed in PHEM buffer and post-fixed in a 0.5% osmic acid for 2 h in the dark and at room temperature. After two rinses in PHEM buffer, the cells were dehydrated in a graded series of ethanol solutions (30–100%). The cells were embedded in EmBed 812

using an Automated Microwave Tissue Processor for Electronic Microscopy, Leica EM AMW. Thin sections (70 nm; Leica-Reichert Ultracut E) were collected at different levels of each block. These sections were counterstained with uranyl acetate 1.5% in 70% Ethanol and lead citrate and observed using a Tecnai F20 transmission electron microscope at 200KV (CoMET facility, MRI facility).

TER measurements

The TER of the iPSc-derived RPE cultured on inserts was measured using the Epithelial Volt/Ohm Meter EVOM2 (World Precision Instruments, Hertfordshire, U.K.). Briefly, electrodes were sterilized in 70% ethanol for 5 min, rinsed and equilibrated in medium, then placed in the compartmentalised chambers with the longer electrode vertically touching the bottom of the dish in the lower chamber and the shorter electrode in the upper chamber without touching the cell layer. TER was recorded once the value stabilised, approximately 5 seconds after placing the electrode. TER values are represented as Ω/cm^2 after subtraction of the background value of a Matrigel-coated transwell filter without cells and multiplication by the growth surface area. Final TER values represent the average measure of three independent filters.

In vitro prenylation assays

Cells were washed in cold PBS, scraped in PBS containing anti-proteases, pelleted and resuspended in cold, freshly prepared, degassed prenylation lysis buffer and the unprenylated cytosolic Rab pool was analysed as previously described (10). Briefly, the freshly prepared lysate was incubated with 9 µM biotin-labelled geranyl pyrophosphate (B-GPP; Euromedex, Souffelweyersheim, France), 22 µM GDP, 70 ng/µl recombinant REP1 (Euromedex) and 80 ng/µl recombinant RGGTase II (Euromedex) at 37°C for 1 h (21,22). The prenylation reaction was stopped with 5x Laemmli's sample buffer containing β-mercaptoethanol (Sigma-Aldrich), boiled at 95°C for 5 min and biotin incorporation analysed by western blot using a 1:5000 HRP-conjugated streptavidin (Jackson ImmunoResearch, Cambridge, Great Britain). The amount of biotinylated Rab proteins was then quantified using Image J software and expressed as a function of the β-actin signal.

Statistical analyses

Due to small sample sizes, statistical analyses were performed using non-parametric tests. In the case of two experimental groups, analyses were performed using a Mann and Whitney test. In the case of three or more experimental groups, global analyses were performed using a Kruskal Wallis ANOVA and post-hoc 2x2 comparisons using a Mann and Whitney test.

Acknowledgements

The authors thank Audrey Senechal (Neurogenetic facility, INM) for help with sequencing analysis, Pauline Bouret and Franck Pellestor (Chromostem facility, CHRU Montpellier) for karyotype analyses, Hassan Boukhaddaoui (MRI facility) for confocal microscopy image analyses, and Chantal Cazevieuille (CoMET, MRI facility) for electron microscopy processing and expertise. The authors also thank Marie-Alice Kong-Hap for primer design,

Pierre Bercier for qPCR experiments, and Christel Vaché and David Baux (CHRU Montpellier) for helpful discussions.

Conflict of Interest statement. None declared.

Funding

This work was funded by the patient associations France Choroideremia, Asociacion de Afectados Coroideremia (Spain), AFM, Retina France and the Federation des Aveugles de France, and by the European Union Seventh Framework Programme (FP7-People-2012-ITN) under grant agreement 317472 (EyeTN).

References

- Berger, W., Kloeckener-Gruissem, B. and Neidhardt, J. (2010) The molecular basis of human retinal and vitreoretinal diseases. *Prog. Retin. Eye Res.*, **29**, 335–375.
- Smith, A.J., Bainbridge, J.W. and Ali, R.R. (2012) Gene supplementation therapy for recessive forms of inherited retinal dystrophies. *Gene Ther.*, **19**, 154–161.
- Bainbridge, J.W., Smith, A.J., Barker, S.S., Robbie, S., Henderson, R., Balaggan, K., Viswanathan, A., Holder, G.E., Stockman, A., Tyler, N. et al. (2008) Effect of gene therapy on visual function in Leber's congenital amaurosis. *N. Engl. J. Med.*, **358**, 2231–2239.
- Maguire, A.M., Simonelli, F., Pierce, E.A., Pugh, E.N., Jr., Mingozzi, F., Bennicelli, J., Banfi, S., Marshall, K.A., Testa, F., Surace, E.M. et al. (2008) Safety and efficacy of gene transfer for Leber's congenital amaurosis. *N. Engl. J. Med.*, **358**, 2240–2248.
- Ghazi, N.G., Abboud, E.B., Nowilaty, S.R., Alkuraya, H., Alhommadi, A., Cai, H., Hou, R., Deng, W.T., Boye, S.L., Almaghamsi, A. et al. (2016) Treatment of retinitis pigmentosa due to MERTK mutations by ocular subretinal injection of adeno-associated virus gene vector: results of a phase I trial. *Hum. Genet.*, **135**, 327–343.
- MacLaren, R.E., Groppe, M., Barnard, A.R., Cottrill, C.L., Tolmachova, T., Seymour, L., Clark, K.R., During, M.J., Cremers, F.P., Black, G.C. et al. (2014) Retinal gene therapy in patients with choroideremia: initial findings from a phase 1/2 clinical trial. *Lancet*, **383**, 1129–1137.
- Kalatzis, V., Hamel, C.P. and MacDonald, I.M. and First International Choroideremia Research, S. (2013) Choroideremia: towards a therapy. *Am. J. Ophthalmol.*, **156**, 433–437. e433.
- van Bokhoven, H., van den Hurk, J.A., Bogerd, L., Philippe, C., Gilgenkrantz, S., de Jong, P., Ropers, H.H. and Cremers, F.P. (1994) Cloning and characterization of the human choroideremia gene. *Hum. Mol. Genet.*, **3**, 1041–1046.
- Andres, D.A., Seabra, M.C., Brown, M.S., Armstrong, S.A., Smeland, T.E., Cremers, F.P. and Goldstein, J.L. (1993) cDNA cloning of component A of Rab geranylgeranyl transferase and demonstration of its role as a Rab escort protein. *Cell*, **73**, 1091–1099.
- Cereso, N., Pequignot, M.O., Robert, L., Becker, F., De Luca, V., Nabholz, N., Rigau, V., De Vos, J., Hamel, C.P. and Kalatzis, V. (2014) Proof of concept for AAV2/5-mediated gene therapy in iPSc-derived retinal pigment epithelium of choroideremia patients. *Mol. Ther. Methods Clin. Dev.*, **1**, 14011.
- Moosajee, M., Ramsden, S.C., Black, G.C., Seabra, M.C. and Webster, A.R. (2014) Clinical utility gene card for: choroideremia. *Eur. J. Hum. Genet.*, **22**, doi: 10.1038/ejhg.2013.183
- Freund, P.R., Sergeev, Y.V. and MacDonald, I.M. (2016) Analysis of a large choroideremia dataset does not suggest a preference for inclusion of certain genotypes in future trials of gene therapy. *Mol. Genet. Genomic Med.*, **4**, 344–358.
- Sergeev, Y.V., Smaoui, N., Sui, R., Stiles, D., Gordiyenko, N., Strunnikova, N. and Macdonald, I.M. (2009) The functional effect of pathogenic mutations in Rab escort protein 1. *Mutat. Res.*, **665**, 44–50.
- Esposito, G., De Falco, F., Tinto, N., Testa, F., Vitagliano, L., Tandurella, I.C., Iannone, L., Rossi, S., Rinaldi, E., Simonelli, F. et al. (2011) Comprehensive mutation analysis (20 families) of the choroideremia gene reveals a missense variant that prevents the binding of REP1 with Rab geranylgeranyl transferase. *Hum. Mutat.*, **32**, 1460–1469.
- Sanchez-Alcudia, R., Garcia-Hoyos, M., Lopez-Martinez, M.A., Sanchez-Bolivar, N., Zurita, O., Gimenez, A., Villaverde, C., Rodrigues-Jacy da Silva, L., Corton, M., Perez-Carro, R. et al. (2016) A Comprehensive Analysis of Choroideremia: From Genetic Characterization to Clinical Practice. *PLoS One*, **11**, e0151943.
- Sonoda, S., Spee, C., Barron, E., Ryan, S.J., Kannan, R. and Hinton, D.R. (2009) A protocol for the culture and differentiation of highly polarized human retinal pigment epithelial cells. *Nat. Protoc.*, **4**, 662–673.
- Seabra, M.C., Mules, E.H. and Hume, A.N. (2002) Rab GTPases, intracellular traffic and disease. *Trends Mol. Med.*, **8**, 23–30.
- Ramsden, S.C., O'Grady, A., Fletcher, T., O'Sullivan, J., Hart-Holden, N., Barton, S.J., Hall, G., Moore, A.T., Webster, A.R. and Black, G.C. (2013) A clinical molecular genetic service for United Kingdom families with choroideraemia. *Eur. J. Med. Genet.*, **56**, 432–438.
- Nabholz, N., Lorenzini, M.C., Bocquet, B., Lacroux, A., Faugere, V., Roux, A.F., Kalatzis, V., Meunier, I. and Hamel, C.P. (2016) Clinical evaluation and cone alterations in choroideremia. *Ophthalmology*, **123**, 1830–1832.
- Alexandrov, K., Horiuchi, H., Steele-Mortimer, O., Seabra, M.C. and Zerial, M. (1994) Rab escort protein-1 is a multifunctional protein that accompanies newly prenylated rab proteins to their target membranes. *embo J.*, **13**, 5262–5273.
- Wu, Y.W., Alexandrov, K. and Brunsfeld, L. (2007) Synthesis of a fluorescent analogue of geranylgeranyl pyrophosphate and its use in a high-throughput fluorometric assay for Rab geranylgeranyltransferase. *Nat. Protoc.*, **2**, 2704–2711.
- Nguyen, U.T.T., Wu, Y., Goodall, A. and Alexandrov, K. (2010) Analysis of protein prenylation in vitro and in vivo using functionalized phosphoisoprenoids. *Curr. Protoc. Protein Sci.*, **62**, 14.13.11–14.13.15.